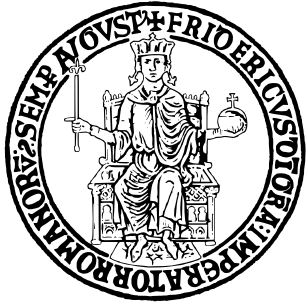


UNIVERSITÀ DEGLI STUDI DI NAPOLI FEDERICO II



SCUOLA POLITECNICA E DELLE SCIENZE DI BASE

DIPARTIMENTO DI INGEGNERIA ELETTRICA E TECNOLOGIE DELL'INFORMAZIONE

NONLINEAR DYNAMICS AND CONTROL

APPLYING NONLINEAR CONTROL TO GOODWIN OSCILLATORS FOR CIRCADIAN RHYTHM TRACKING IN NEUROSPORA

Component
Roberto Rocco

Academic Year 2024–2025

Contents

1	Dynamic Model	2
1.1	Circadian cycle	2
1.2	Goodwin oscillator	3
2	Open-loop analysis	4
2.1	Phase-plane analysis	4
2.2	Proof of the existence of a limit cycle	5
2.3	Open-Loop behavior	7
3	Synthesis	8
3.1	Control input and requirements	8
3.2	Linear control synthesis	9
3.3	I/O Feedback Linearization	17
3.4	Sliding Mode Control	26
4	Comparison	36

Introduction

The **Goodwin oscillator** represents a simplified yet paradigmatic model of a biochemical system characterized by a stable **limit cycle**. It is widely used to describe phenomena such as circadian rhythms, hormonal cycles, and self-oscillatory metabolic pathways. In this class of systems, oscillations can emerge either periodically or aperiodically. Regardless of their nature, it is always possible to apply control to synchronize the natural oscillations of the system with the desired ones, a process known as **entrainment**.

The mathematical treatment of entrainment phenomena, particularly those involving nonlinear interactions induced by periodic exogenous signals, remains an open problem. In this context, the following study investigates the nature of the oscillations present in the specific **Goodwin oscillator** being considered. Subsequently, control techniques of both **linear** and **nonlinear** types are applied. In the chapters of the article, the following topics are presented:

1. Circadian Cycle and Dynamic Model

This chapter discusses the phenomenon of the circadian cycle and introduces the dynamic model that describes it.

2. Open-Loop System Analysis

This chapter presents an open-loop analysis of the system, demonstrating the existence of limit cycles through the use of a Poincaré map.

3. Control Techniques

In this chapter, one linear control technique and two nonlinear control techniques are applied to the system. A robustness and disturbance rejection analysis is finally performed.

Chapter 1

Dynamic Model

In the first chapter, the functioning of a circadian cycle is briefly explained in general terms, followed by the presentation of the dynamic model of the circadian cycle in *Neurospora*.

1.1 Circadian cycle

The circadian cycle is an internal biological system that regulates the physiological and behavioral processes of living organisms, synchronizing them with the day-night alternation. Circadian rhythms regulate important functions in the human body, such as:

- Sleep patterns
- Hormone release
- Appetite and digestion
- Body temperature

Circadian rhythms are governed by a **circadian clock**: it acts as master clock, required for coordination of biological processes so that they occur at the correct time, maximizing an individual's fitness. In mammals, this clock is located in the **suprachiasmatic nucleus** (SCN), a group of cells located in the hypothalamus. For example, the SCN controls the production of the hormone melatonin based on the amount of light perceived by the eyes. In the evening, the master clock signals the brain to increase melatonin production, inducing sleepiness.

Going deeper into the physiological processes regulating the cycle, the SCN controls the expression of circadian genes. The main role is played by the **mRNA**, which is the intermediate molecule that carries these instructions for **protein** production from the DNA to the ribosomes, where protein synthesis takes place. The SCN's regulation of mRNA concentration ensures an oscillatory behavior for this molecule, which results in an oscillatory pattern in protein concentration as well. Finally, proteins form complexes that inhibit their own transcription. This mechanism enables **negative feedback**, and their degradation allows the cycle to restart.

Light and dark have the greatest influence on circadian rhythms, as the SCN receives illumination information through the eyes: given the possibility to control. Given the ability to regulate **luminous exposure**, the oscillatory properties of the **circadian oscillator** can be adjusted. By varying the intensity, duration and frequency of luminous exposure, the **phase response curve** (PRC) governing the oscillator can be modified, influencing its intrinsic period (T), amplitude (A), and phase (ϕ). This mechanism takes the name of *entrainment*: it plays an important role in the functioning of living organisms, adapting them to the changing environment.

In the following, the circadian cycle of *Neurospora* (a type of fungus) will be considered. The reason for this choice is the representative simplicity that can be applied to this cycle. However, the significance of the study can be easily generalized to cycles observed in other living species.

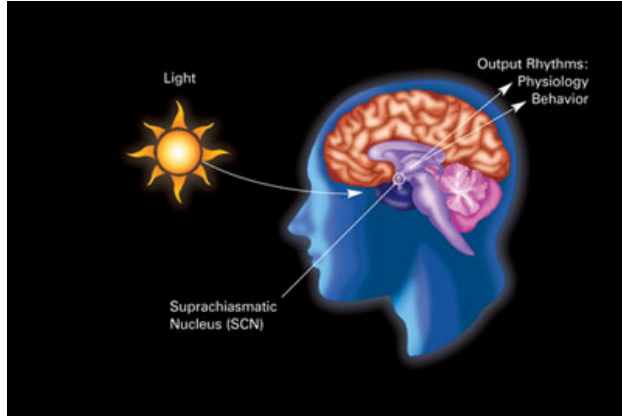


Figure 1.1: Circadian rhythm stimulated by light

1.2 Goodwin oscillator

To model the circadian rhythm of a Neurospora, the **Goodwin oscillator** has been taken into account: it is a minimal model that describes the oscillatory negative feedback regulation of a translated protein which inhibits its own transcription. A three-dimensional Goodwin oscillator exposed to constant light u is established as follows:

$$\begin{cases} \frac{dX}{dT} = \frac{1}{1+bZ^n} - k_1 X + u, \\ \frac{dY}{dT} = X - k_2 Y, \\ \frac{dZ}{dT} = Y - k_3 Z. \end{cases} \quad (1.1)$$

where X , Y and Z represent the concentrations of clock gene mRNA, protein and an inhibitor, respectively. The Hill coefficient n , characterizing the degree of cooperativity of the repression process, has been found to be necessary and sufficient to generate robust limit-cycle oscillations. It has been proved that stable limit-cycle oscillation can occur only when the Hill coefficient is $n > 8$. Accordingly, the Hill coefficient was assumed to be $n = 9$ throughout this article, while $b = 1$. k is the degradation rate for X , Y and Z respectively. This value has been set at $k = 0.1$ (for all the states). For simplicity, we let $t = kT$, $x = k^{-2}X$, $y = k^{-1}Y$, and $z = Z$, and then Eq. (1.1) can be reduced to:

$$\begin{cases} \frac{dx}{dt} = \frac{\alpha}{1+z^n} - x + \alpha u, \\ \frac{dy}{dt} = x - y, \\ \frac{dz}{dt} = y - z, \end{cases} \quad (1.2)$$

where $\alpha \equiv k^{-3}$. All terms are linear except the repression term $\frac{\alpha}{1+z^n}$ described by the Hill function. The power of this reduction is that all parameters (α , Hill coefficient n , and light intensity u) appear only in the first equation of Eq. (1.2). Without special statement, the numerical simulations and the mathematical analysis were performed on the basis of Eq. (1.2)

Chapter 2

Open-loop analysis

In this chapter the open-loop analysis of the Goodwin oscillator will be carried out. First, the open loop trajectory of the system will be analyzed, then the stability of the limit cycle will be studied via Poincare theory.

2.1 Phase-plane analysis

First, possible equilibrium points were sought in the system. The equilibrium points \mathbf{x}^* are those that satisfy the system of equations:

$$\begin{cases} \frac{\alpha}{1+z^n} - x + \alpha u = 0, \\ x - y = 0, \\ y - z = 0, \end{cases} \quad (2.1)$$

Considering the following typical parameter values: $k = 0.1$, $\alpha = k^{-3} = 0.001$, $n = 9$, $u = 0$, the only equilibrium point results in:

$$\mathbf{x}_{\text{in}} = \begin{bmatrix} 2.64 \\ 2.64 \\ 2.64 \end{bmatrix}$$

To analyze the stability of this point, the jacobian has been evaluated: as was to be expected, the three eigenvalues turn out to be as follows:

$$\mathbf{eig} = \begin{bmatrix} -14.1558 + 0.0000i \\ 5.5779 + 11.3933i \\ 5.5779 - 11.3933i \end{bmatrix}$$

being the first eigenvalue negative, we get (local) stability in one direction, while having the other two a positive real parts results in an exponential divergence in the direction of their eigenvectors. Finally, the imaginary parts indicate oscillatory behavior: the equilibrium point is a *saddle-focus*. This leads us to suspect the existence of a *limit cycle* surrounding this equilibrium point: it is obtained when the nonlinear term starts to counteract the divergence due to the linear terms. The phase plane analysis, conducted using the MATLAB solver *ODE45* (required to plot trajectories induced by three-dimensional vector fields), confirms the existence of such a limit cycle through simulation. In Fig. 2.1, two trajectories rooted in different initial conditions are shown.

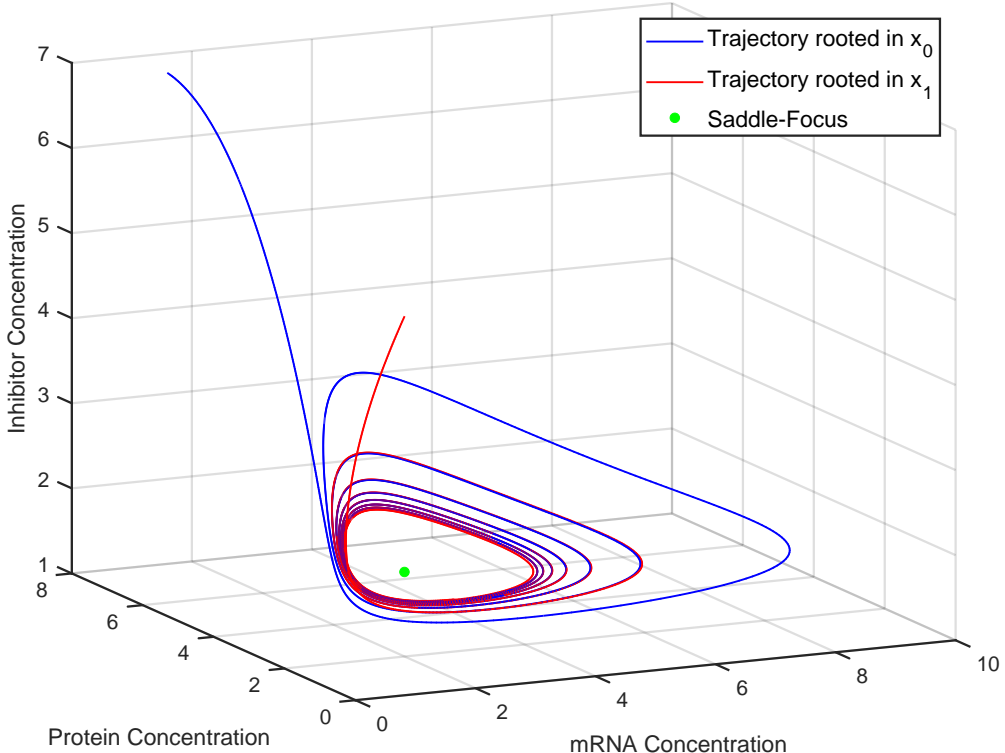


Figure 2.1: 3D trajectory of the system

2.2 Proof of the existence of a limit cycle

The Goodwin oscillator is capable of exhibiting self-sustained oscillation, resulting in a stable limit cycle attractor for the trajectory of the system. Poincaré's theory has been used to demonstrate the existence and stability of the limit cycle.

Given the three-dimensional Goodwin oscillator, to apply Poincaré's method, we must first construct a surface of section, denoted as S . The surface S is required to be transverse to the flow; that is, every trajectory originating on S must flow through it rather than run parallel to it. The *Poincaré map*, P , is a mapping from S onto itself, obtained by following trajectories from one intersection with S to the next. If $x_k \in S$ denotes the k th intersection, then the Poincaré map is defined by

$$x_{k+1} = P(x_k).$$

From this point onward, we study the evolution of trajectories by evaluating the intersections between the original system's trajectories and the Poincaré section, effectively reducing the problem by one dimension.

Importantly, if x^* is a fixed point of P , that is, if $P(x^*) = x^*$, then the trajectory starting at x^* returns to x^* after some time T and is therefore a *closed orbit* of the original system (fixed points are excluded due to the nature of the system).

As the section S , we chose the plane $x_3 = C$, with C appropriately. As can be seen in Fig. 2.3, each oscillation intersects the plane at a single point. Finally, the Poincaré map in Fig. highlights the convergence of trajectories onto a fixed point, thereby demonstrating the existence of a limit cycle in the original system. It should be noted that this map displays both the incoming and outgoing intersections with the plane, while, by running the appropriate code, it is possible to observe the version that highlights only the unidirectional crossings. .

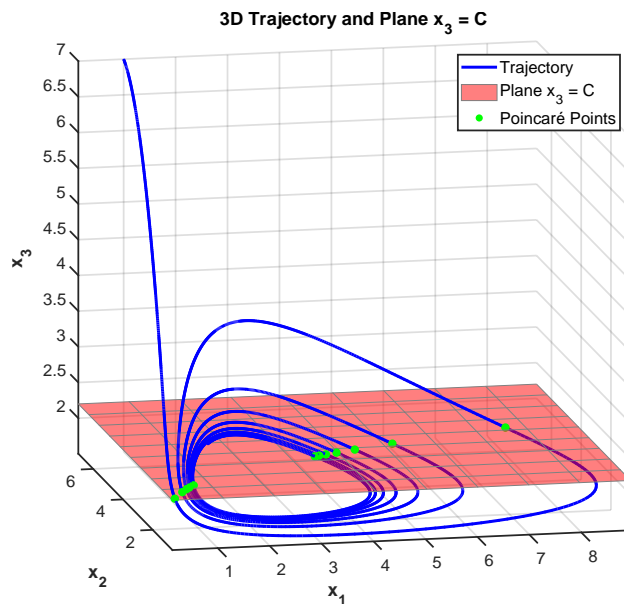


Figure 2.2: Intersection between the Poincaré section and the trajectory

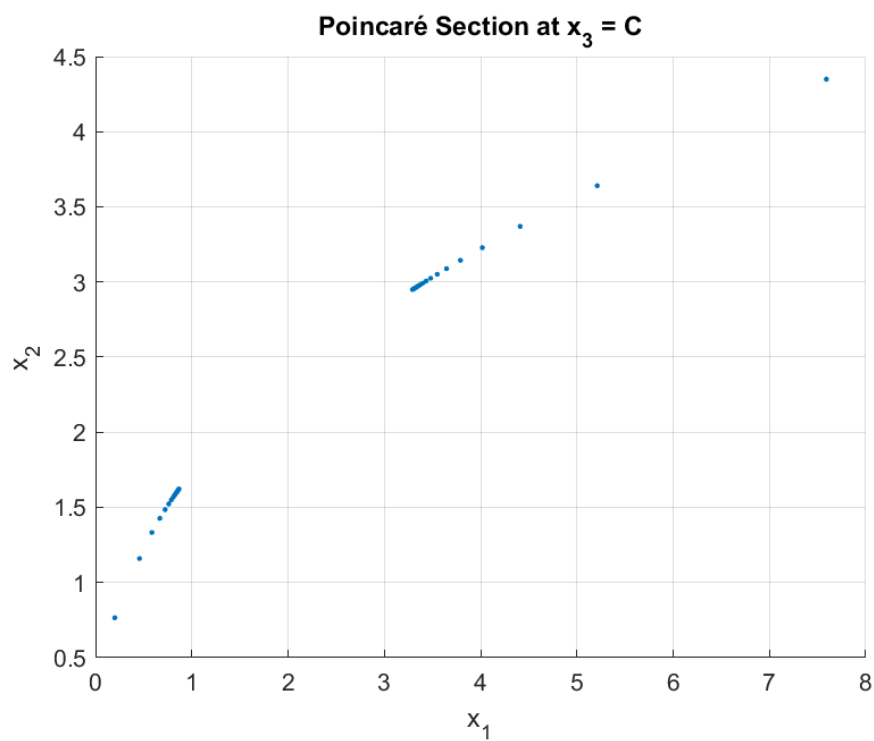


Figure 2.3: Poincaré Map

2.3 Open-Loop behavior

Finally, the open-loop behavior of the system is analyzed. The initial condition chosen is $x_0 = [1; 7; 7]$, while the parameter values are $k = 0.1$, $\alpha = k^{-3} = 0.001$, $n = 9$, and $u = 0$. As can be observed in Fig. 2.4, the concentrations of mRNA, proteins, and inhibitors oscillate continuously, each with its own period and amplitude. Specifically, defining the period as the distance between two successive peaks, they are respectively:

$$T = \begin{bmatrix} 4.0391 \\ 4.0544 \\ 4.0371 \end{bmatrix};$$

regarding the average amplitudes, they are respectively:

$$A = \begin{bmatrix} 4.2157 \\ 3.0109 \\ 2.5785 \end{bmatrix}.$$

As highlighted, the Goodwin oscillator under consideration exhibits periodic oscillations, but the signals themselves are far from a sinusoidal pattern. Moreover, not every peak attains the same value: repetition of values occurs every three peaks.

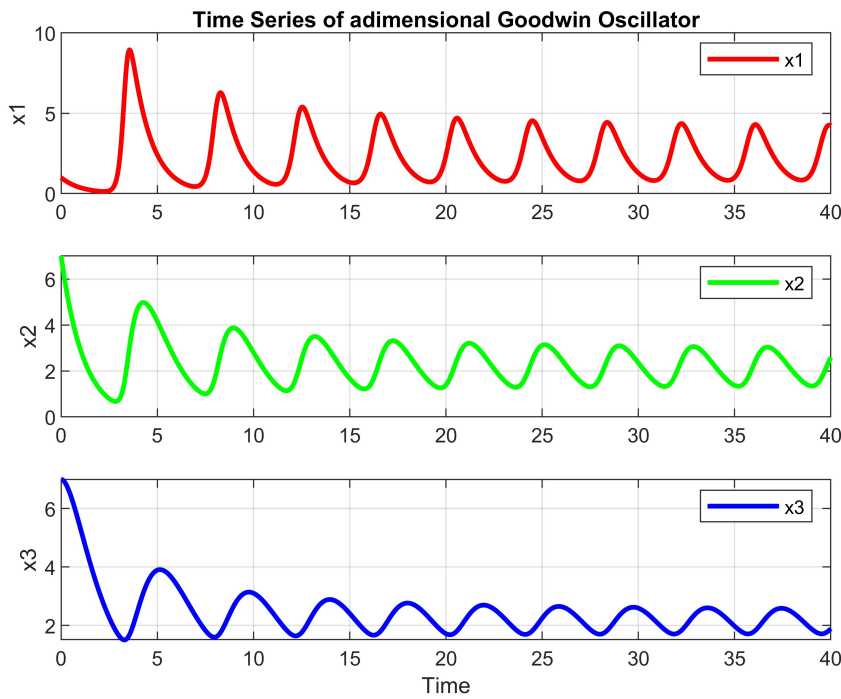


Figure 2.4: Timeseries of mRNA, protein and inhibitor concentration

Chapter 3

Synthesis

Overview

This chapter outlines the design and analysis of control strategies for the system under study. The workflow is organized as follows:

- **Control Input Definition:** The control input for the system is formally defined, and the requirements for the control problem of interest are established.
- **Controller Development:** Three distinct control architectures are implemented:
 1. **Proportional-Integral (PI) Control:** A linear control strategy designed using the linearized system model and subsequently validated on the nonlinear system.
 2. **Input-Output Feedback Linearization (I/O FBL):** A nonlinear control method that algebraically transforms the system dynamics into a linear input-output mapping.
 3. **Sliding Mode Control (SMC):** A robust nonlinear control technique that drives the system trajectories toward a predefined sliding manifold.
- **Robustness Analysis:** Each controller is subjected to a robustness test to evaluate its performance under:
 - Parametric uncertainties (e.g., deviations in model parameters).
 - External disturbances (e.g., additive noise or unmodeled dynamics).

The chapter systematically bridges theoretical design to practical implementation, emphasizing robustness and adaptability in nonlinear control systems.

3.1 Control input and requirements

To properly define a reference with a physical meaning for x_1 , we refer to the open-loop behavior presented in Section 2.3. As shown, the oscillations of this variable are irregular and differ significantly from those of a sinusoid. The aim of this study is to demonstrate that, with a suitable input, it is possible to regularize the oscillations of mRNA concentration, making their behavior closer to that of a sinusoid.

The comparison between the chosen reference and the open-loop behavior is illustrated in Fig. 3.1. The values used to generate the sinusoidal reference are as follows:

$$\text{Ampdes} = A = 2.2, \quad \text{Freqdes} = F = \frac{2\pi}{6}, \quad \text{Phasedes} = \phi = \frac{3\pi}{2}, \quad \text{Biasdes} = B = 3.3.$$

The role of the various controller is to follow a sinusoidal signal (unless otherwise specified) in the form $A \cdot \sin(F \cdot t + \phi) + B$.

For all the control strategies presented below, the requirements are as follows:

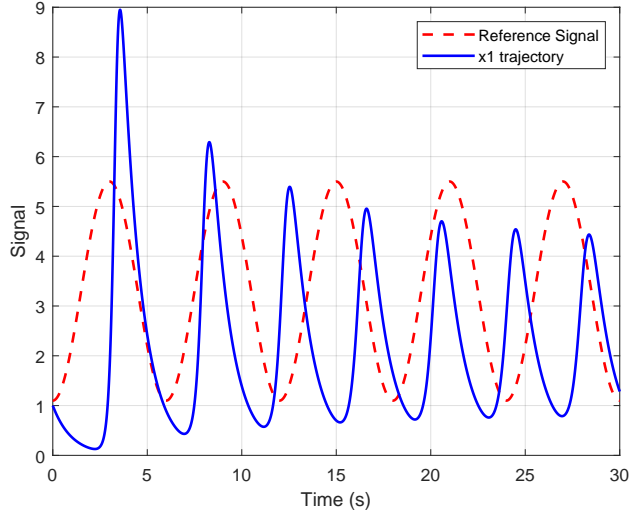


Figure 3.1: Reference and Trajectory of x_1 compared.

- The desired value for the mRNA concentration is given by the sinusoidal reference shown in Fig. 3.1.
- The settling time, defined as the time t_s after which the absolute error $|e(t)|$ remains within a prescribed bound ($|e(t)| < 0.05 \cdot \max_t |e(t)|$), should be minimized. More than 2 seconds are considered failed test
- The control input must be bounded within a specified range, that is $[-9, 9] \times 10^{-3}$.

3.2 Linear control synthesis

To linearize a nonlinear system in the neighborhood of an equilibrium x_{eq} , first determine the equilibrium by solving

$$f(x_{\text{eq}}) = 0.$$

Next, compute the Jacobian matrix J of the system by taking the partial derivatives of $f(x)$ with respect to x and evaluating it at x_{eq} ; finally, its possible to express the system in terms of the deviation from the equilibrium, $\delta x = x - x_{\text{eq}}$, and approximate the dynamics using a first-order Taylor expansion, yielding the linearized model

$$\dot{\delta x} \approx J(x_{\text{eq}}) \delta x.$$

This approximation captures the local behavior around the equilibrium while neglecting higher-order nonlinear terms.

The only caution to be taken before switching to the linear system is as follows. When linearizing around an equilibrium point $(x_{\text{eq}}, u_{\text{eq}})$, it is important to account for both the state and the input. Define the deviations

$$\delta x = x - x_{\text{eq}} \quad \text{and} \quad \delta u = u - u_{\text{eq}}.$$

The linearized model then takes the form

$$\dot{\delta x} \approx A \delta x + B \delta u,$$

where

$$A = \left. \frac{\partial f}{\partial x} \right|_{(x_{\text{eq}}, u_{\text{eq}})} \quad \text{and} \quad B = \left. \frac{\partial f}{\partial u} \right|_{(x_{\text{eq}}, u_{\text{eq}})}.$$

In the considered case the linearization is performed in the neighborhood of the equilibria x_{eq} discussed in 2.1, that is the one obtained in open loop, i.e, when $u = u_{\text{eq}} = 0$. The scheme in Fig. 3.2 shows the system linearized at the equilibrium point x_{eq} , which, as mentioned, is a saddle-focus.

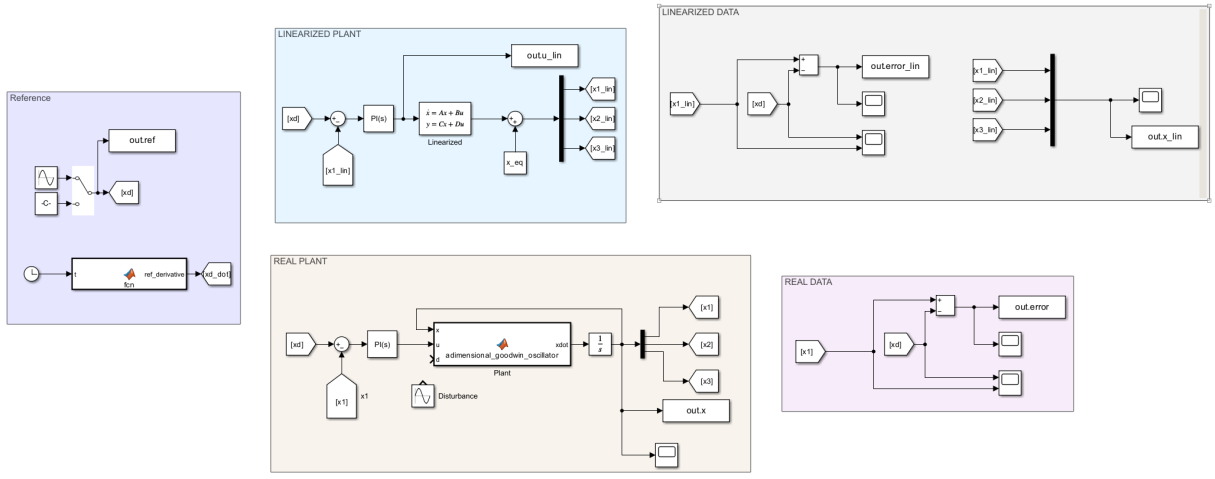


Figure 3.2: Simulink scheme of linearized system

After obtaining the system linearized around the equilibrium, we can proceed with the control design. In the scheme with the linear controller, the tuning of the PI controller gains is based on the linearized system. For this scheme, neglecting the requirements it is unable to meet, the objective was set to reach a constant reference equal to the average value of the desired sinusoid, starting from a nearby point (which does not deviate significantly from the equilibrium around which the linearization was performed). Finally, an attempt to track a sinusoid is shown, though with an amplitude reduced to one-tenth of the desired value. This decision is justified as follows: the linearized controller is effective only in a neighborhood around the equilibrium, and the originally chosen sinusoidal reference does not remain sufficiently close to this operating point. After different trials, a PI controller has been chosen, whose control gains are $P = 0.01$ and $I = 0.008$. With this choice, the constant reference $x_d = \text{Biasdes} = 3.3$ (the average value of the sinusoid) is correctly reached by both the linearized system and the real model, as shown in the following plots.

Constant reference

Here as reference has been chosen the constant value of 3.3. The initial condition chosen for the simulation is [2.64; 2.64; 2.64], which corresponds to 80% of the reference value the system is intended to reach.

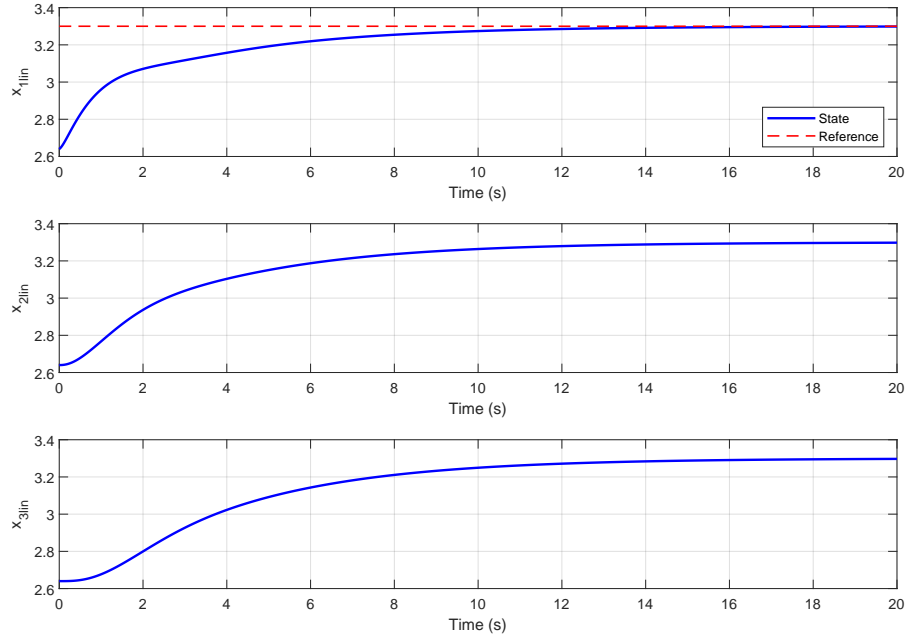


Figure 3.3: State evolution of linearized system.

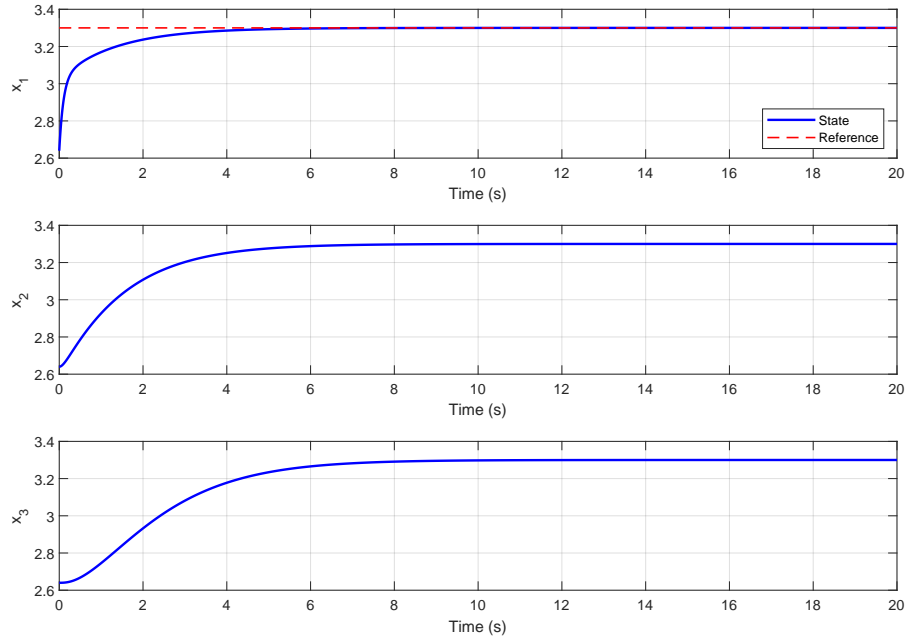


Figure 3.4: State evolution of real system.

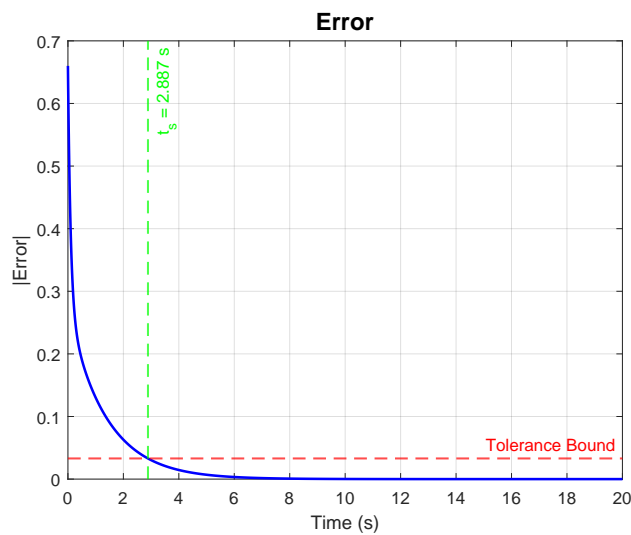


Figure 3.5: Error evolution of real system

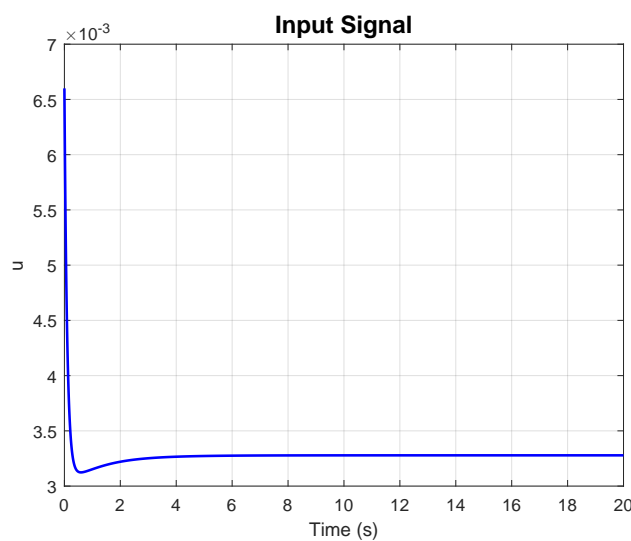


Figure 3.6: Input signal of real system.

As evident, the PI controller, as tuned, is able to meet the specifications, with a bounded input and a settling time of 2.887 seconds.

Sinusoidal reference

Here as reference a sinusoidal signal has been chosen, with a tenth the amplitude of the desired one, by select the right signal with the simulink manual switch. The gain values have been modified and set to $P = 0.015$ and $I = 0.01$. The initial condition remains unchanged, namely [2.64; 2.64; 2.64].

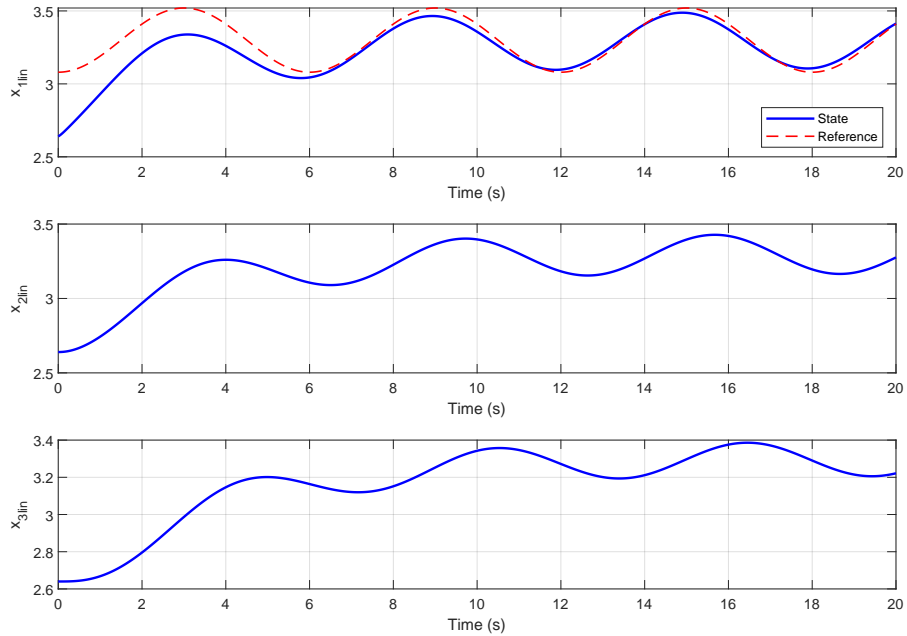


Figure 3.7: State evolution of linearized system.

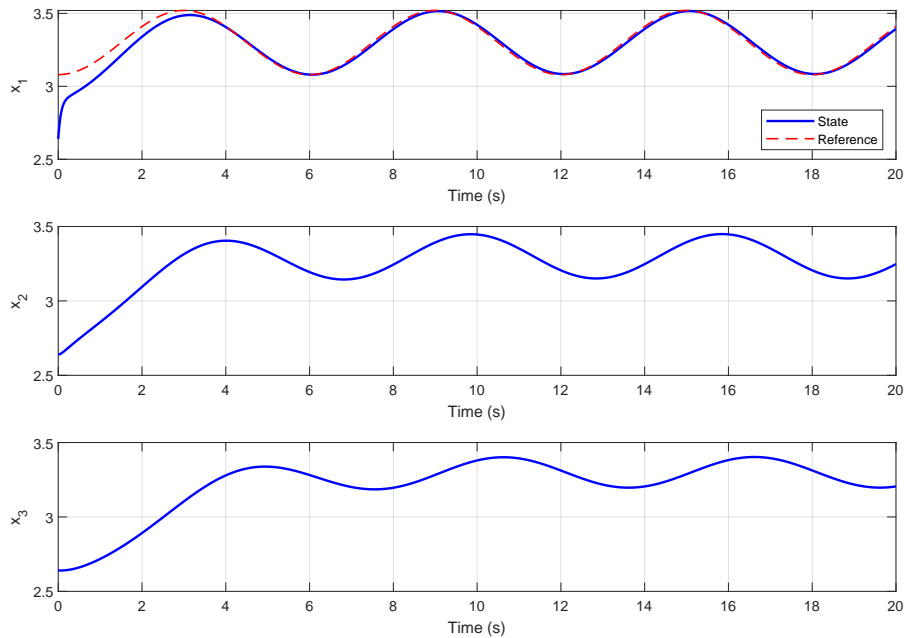


Figure 3.8: State evolution of real system.

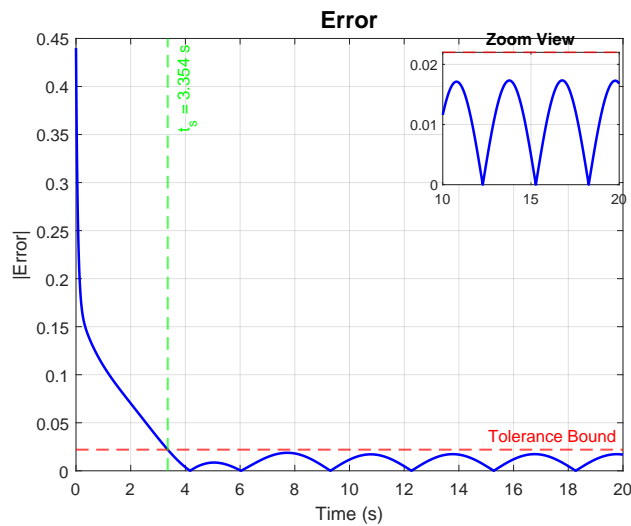


Figure 3.9: Error evolution of real system

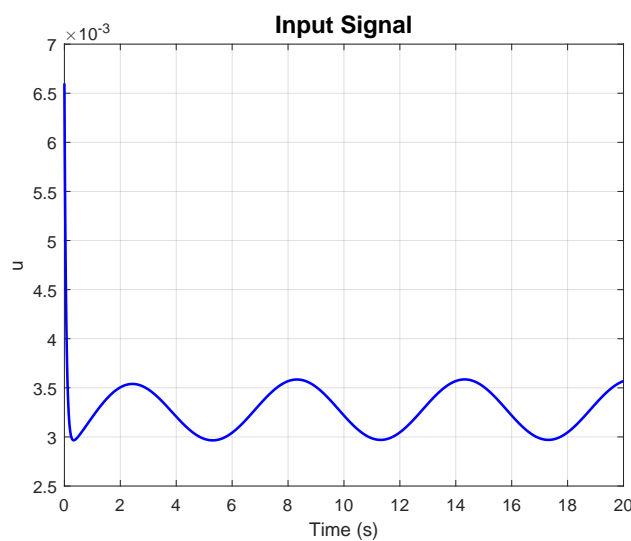


Figure 3.10: Input signal of real system.

As evident, the PI controller, as tuned, is able to meet the tracking specifications, with a bounded input and a settling time of 3.354 seconds.

Disturbance

Here as reference a sinusoidal signal has been chosen, with a tenth the amplitude of the desired one, by select the right signal with the simulink manual switch. The gain values have been modified and set to $P = 0.015$ and $I = 0.01$. The initial condition remains unchanged, namely [2.64; 2.64; 2.64]. A disturbance with intensity equal to that of the input signal has been introduced:

$$Ref = 3.3$$

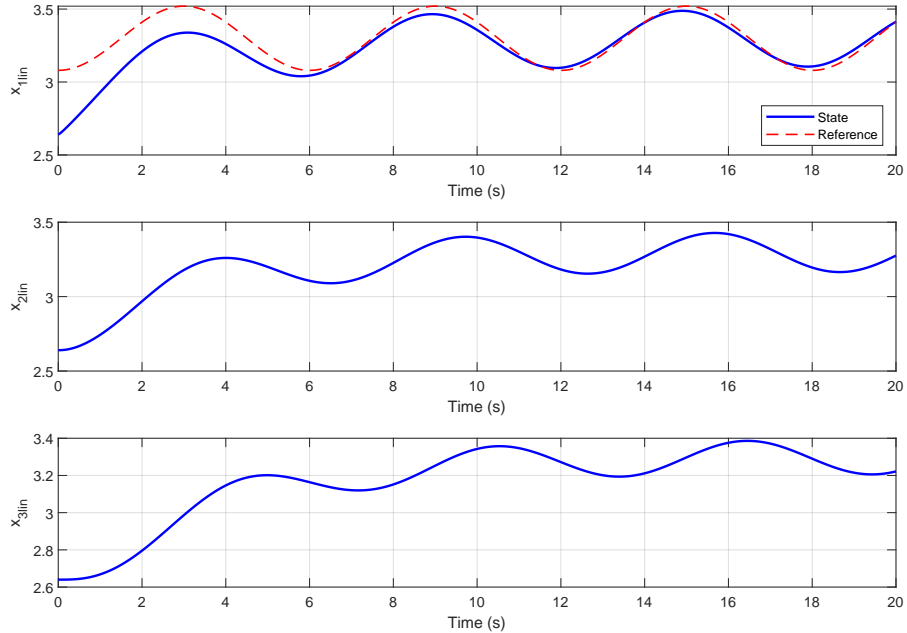


Figure 3.11: State evolution of linearized system.

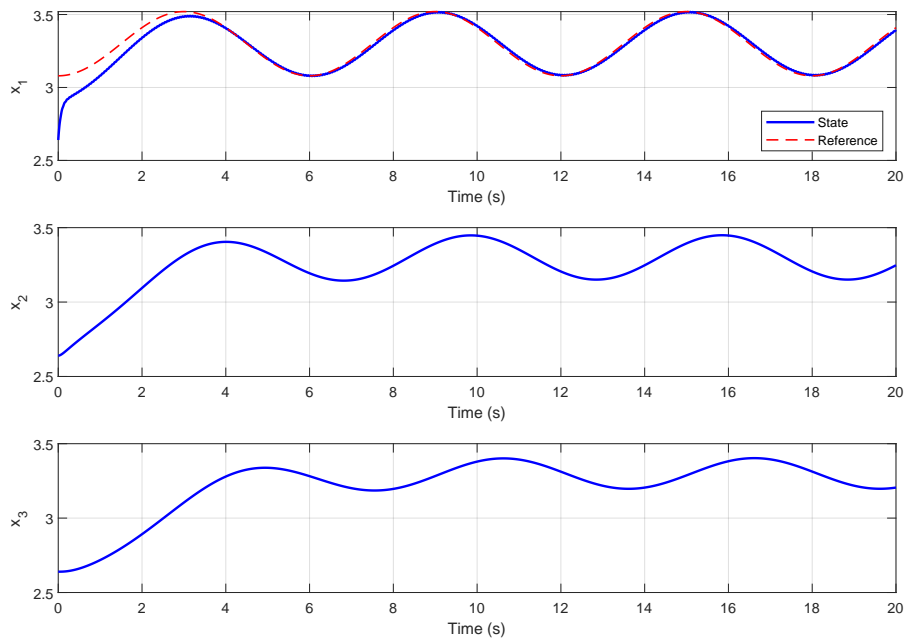


Figure 3.12: State evolution of real system.

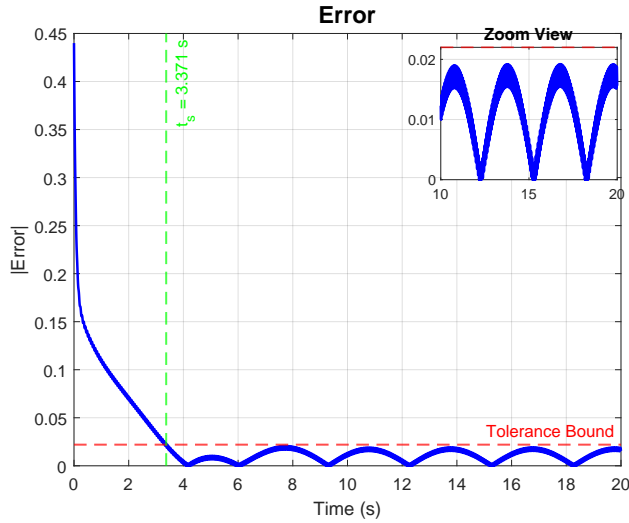


Figure 3.13: Error evolution of real system

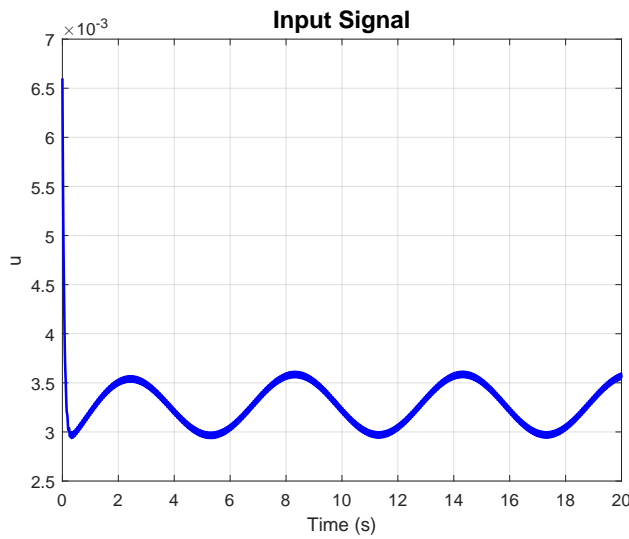


Figure 3.14: Input signal of real system.

Even with such a high disturbance, the linear controller is able to meet the requirements, achieving a settling time of 3.371 seconds. All simulations on the linear system were carried out using modified reference signals, in order to align with the philosophy of the linearized system approximation: its validity holds only in the neighborhood of the equilibrium point x_{eq} . When attempting to follow the original trajectory, the linear controller fails to meet the predefined requirements.

3.3 I/O Feedback Linearization

Input-Output Feedback Linearization is a nonlinear control strategy that involves two control loops. The internal loop aims to globally transform the system into a linear form, while the second loop is a linear controller. The model is rewritten in the affine form:

$$\dot{x} = f(x) + g(x)u, \quad y = h(x), \quad (3.1)$$

where $x \in \mathbb{R}^n$ is the state, $u \in \mathbb{R}^m$ is the input, and $y \in \mathbb{R}^p$ is the output.

The nonlinear system considered is defined by:

$$f(x) = \begin{bmatrix} -x_1 + \frac{a}{1+x_3^n} \\ -x_2 + x_1 \\ -x_3 + x_2 \end{bmatrix}$$

where a, n are constant parameters, while the system output is $y = h(x) = x_1$ and the $g(x) = [a; 0; 0]$. The goal is to transform the system into a linear input-output (I-O) form:

$$y^{(r)} + a_{r-1}y^{(r-1)} + \cdots + a_0y = v,$$

where r is the relative degree, $y^{(i)}$ denotes the i -th derivative of the output, and v is the control input that will be applied on the global linearization of the system. The relative degree r is determined using Lie derivatives. For a system with output $h(x)$, r is the smallest integer such that:

$$\begin{cases} \mathcal{L}_g(\mathcal{L}_f^i(h)) = 0, & i = 0, 1, \dots, r-2, \\ \mathcal{L}_g(\mathcal{L}_f^{r-1}(h)) \neq 0. \end{cases}$$

Here, since $\mathcal{L}_g(h) \neq 0$, the relative degree is $r = 1$, meaning that $n - r = 3 - 1 = 2$ internal dynamic have to be studied. The control input u is designed as:

$$u = \frac{1}{\mathcal{L}_g(h)} [-\mathcal{L}_f(h) + v].$$

We obtain:

$$u = -\frac{1}{a} \left[\frac{a}{1+x_3^n} - x_1 - v \right]$$

The auxiliary input v is chosen as a proportional (P) controller:

$$v = K_P e + K_I \int e dt + \dot{x}_d$$

where $K_P = 10$ is the proportional gain, and y_d is the desired output. Substituting v and $u(t)$ into the system dynamics yields the closed-loop equations:

$$\begin{cases} \dot{x}_1 = v = K_P e + K_I \int e dt + \dot{x}_d, \\ \dot{x}_2 = -x_2 + x_1 \\ \dot{x}_3 = -x_3 + x_2 \end{cases}$$

The first state x_1 is directly controlled by v , leading to exponential convergence of y to y_d due to the P controller. The dynamics of both x_2, x_3 remain unforced: those are internal dynamic, whose stability can be proven by analytical proof. All the discussed equations have been implemented in the scheme in Fig. 3.15

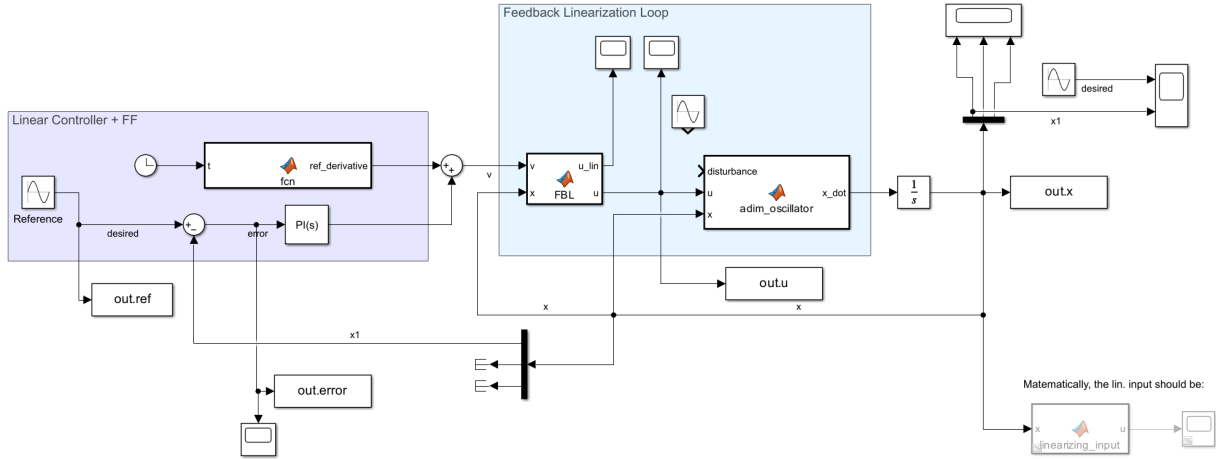


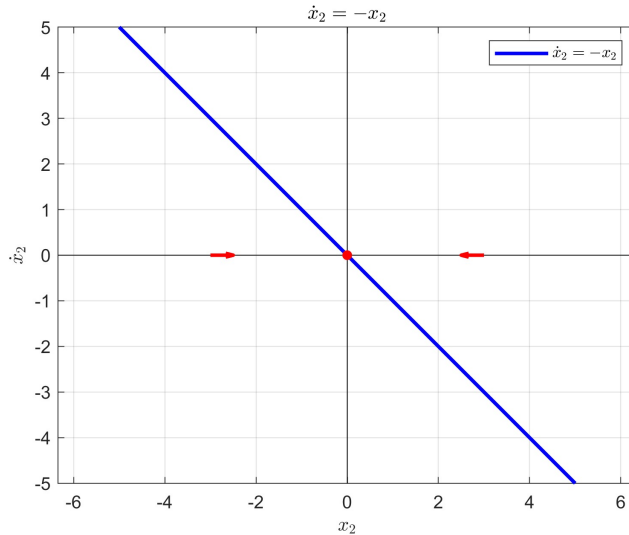
Figure 3.15: FBL scheme

Proof of stability of internal dynamic

Stability is proven only for x_2 : similar proof follows for x_3 . By resuming the dynamics of x_2 , it can be written that

$$\dot{x}_2 = -x_2 + y_d$$

Now, since the reference is of course bounded, this equation can be seen as a dynamical system forced by a bounded input. To prove its asymptotic stability (which imply the BIBO's one), its sufficient to note that the system has an equilibrium point at $(0, 0)$. If $x_2 > 0$, its derivative satisfies $\dot{x}_2 < 0$, so the trajectory moves towards the origin. Similarly, if $x_2 < 0$, then $\dot{x}_2 > 0$, meaning the trajectory again moves towards the origin, as can be seen in Fig. 3.16

Figure 3.16: Internal stability of x_2

Performance

In the following, the time evolutions of the state x , the control input u , and the error are shown. Notice that the tracking of the desired trajectory is almost perfect, meaning that in Fig. 3.17 the trajectory x_1 is overlaid on x_d . Initial condition is set to $x_0 = [1; 7; 7]$.

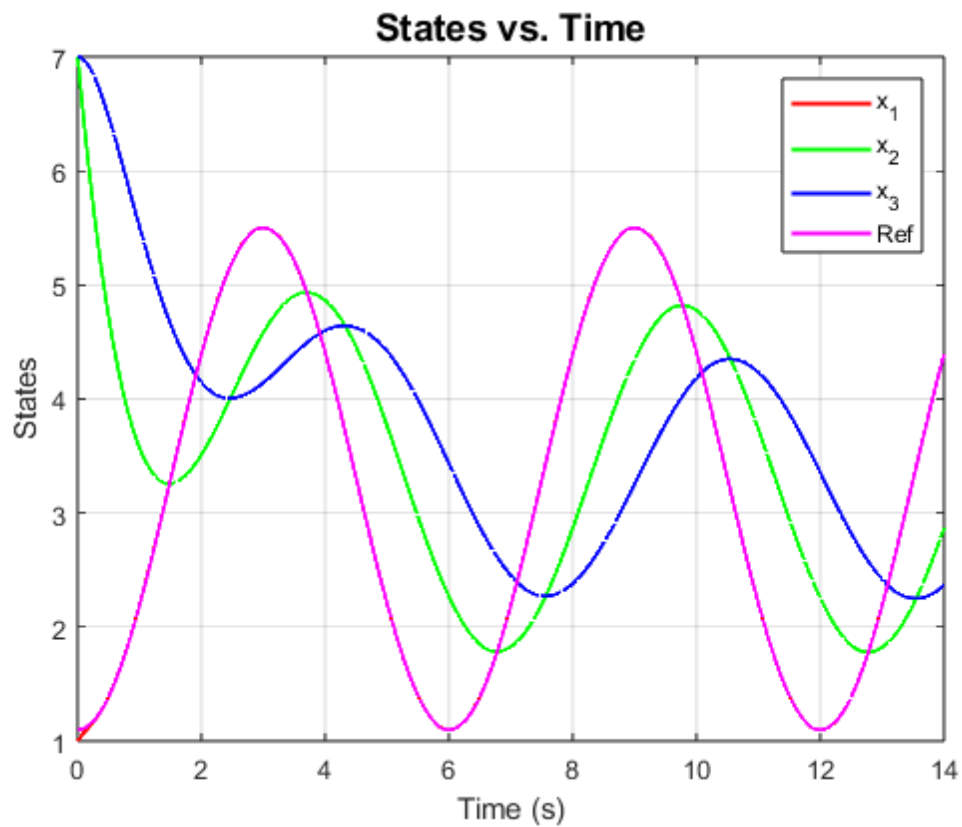


Figure 3.17: State evolution with FBL scheme

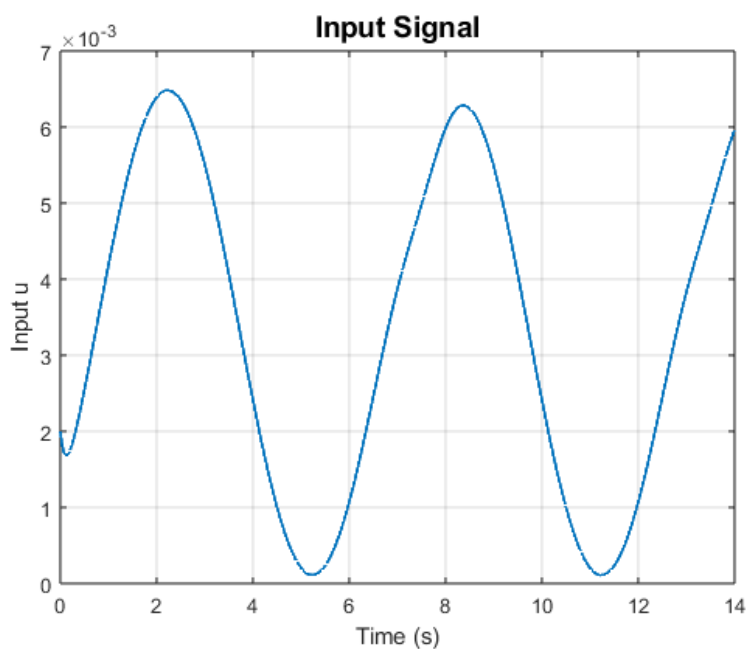


Figure 3.18: Control amplitude with FBL scheme (peak: 0.0064)

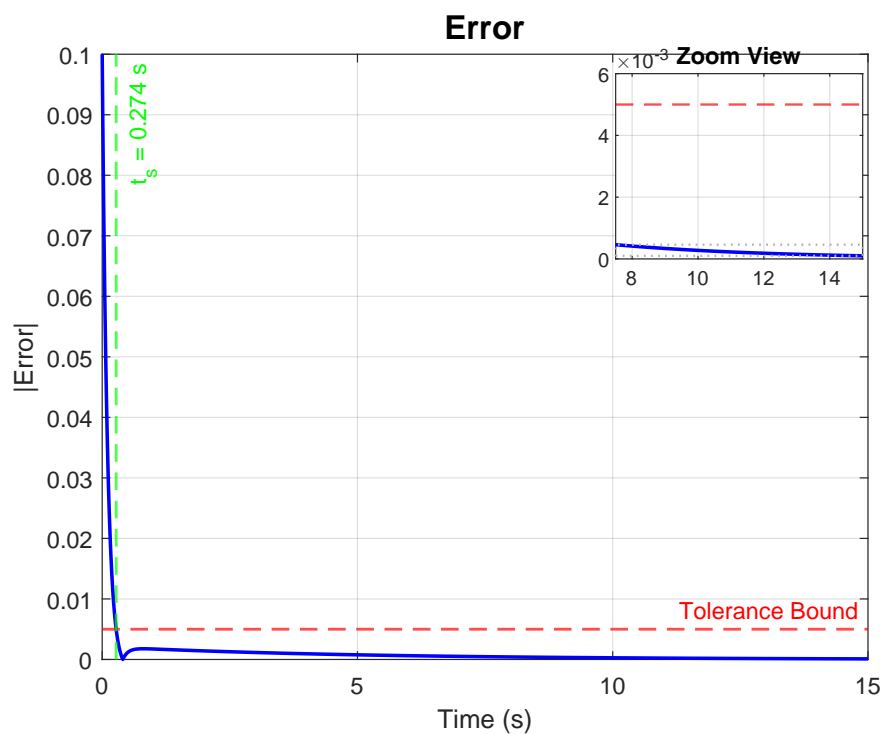


Figure 3.19: Error dynamic with FBL scheme (settling time: 0.274 seconds)

Disturbance

Disturbance has been set with an amplitude one-tenth of the desired, with a frequency a hundred times of the desired one (see Sec. 3.1 for parameters value):

$$d = \frac{A}{10} \sin(100 \cdot F \cdot t + \phi)$$

As can be seen, disturbance affects overall performance, causing high frequency oscillation in the error dynamic. The overall tracking capability is still acceptable. The higher the amplitude, the worst will be the performance. Simulation time has been decreased to 10 seconds to better appreciate the disturbance effects.

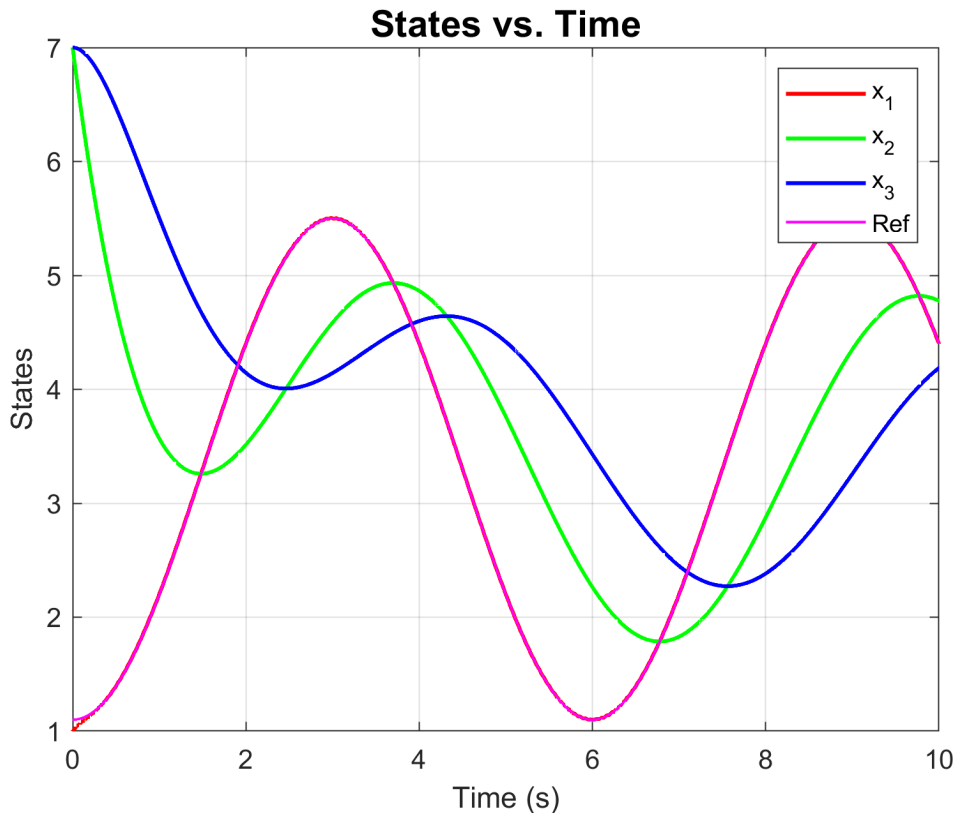


Figure 3.20: State evolution FBL scheme with disturbance

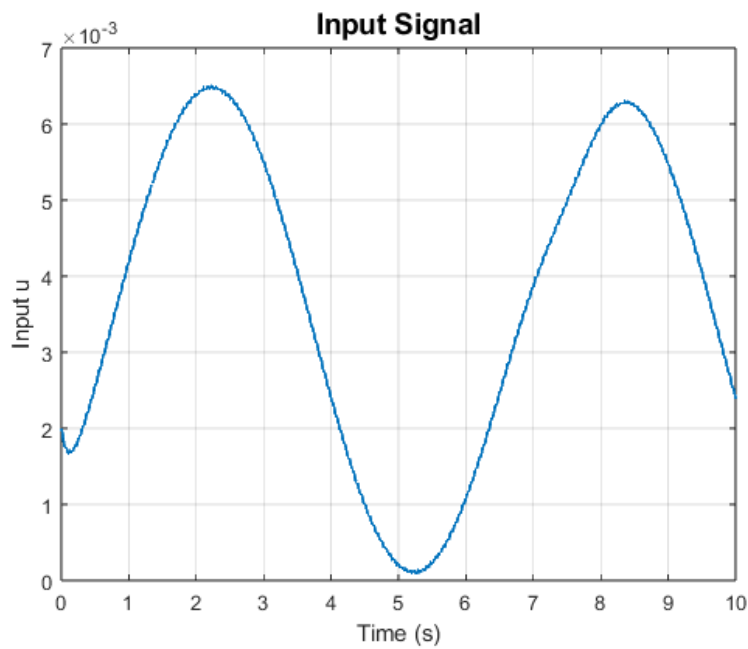


Figure 3.21: Control amplitude FBL scheme with disturbance

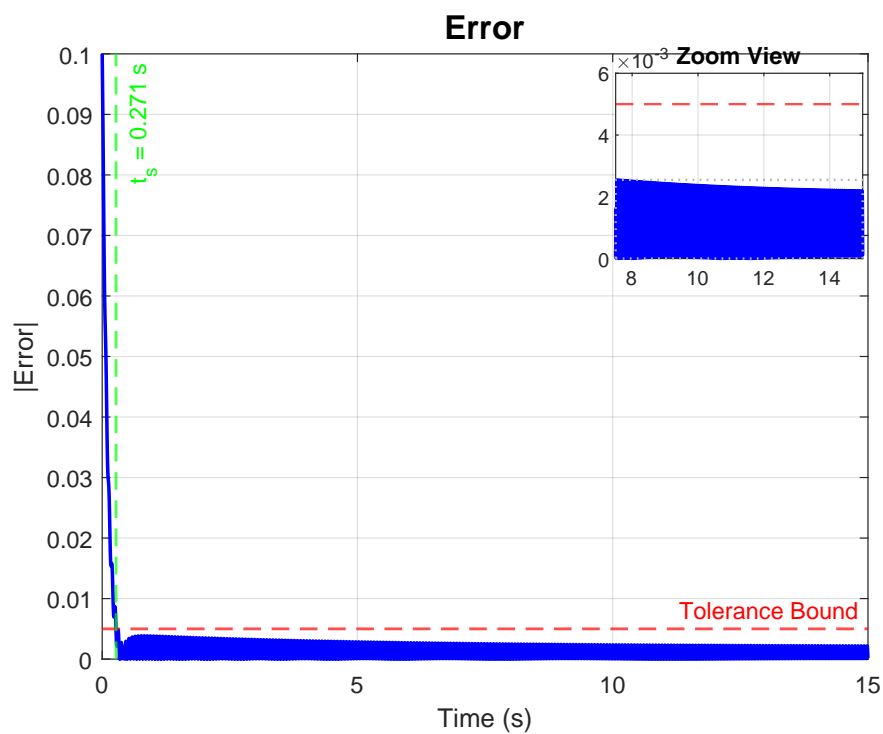


Figure 3.22: Error dynamic FBL scheme with disturbance (settling time: 0.271 seconds)

Robustness

To check robustness of the scheme to parameter uncertainties, ten simulations have been launched, with a randomic parameter variation, up to 50% of their nominal value. Finally, for one of these 10 simulations, the input and error are reported. Remember that in the dynamic model,

$$a = b^{-3}$$

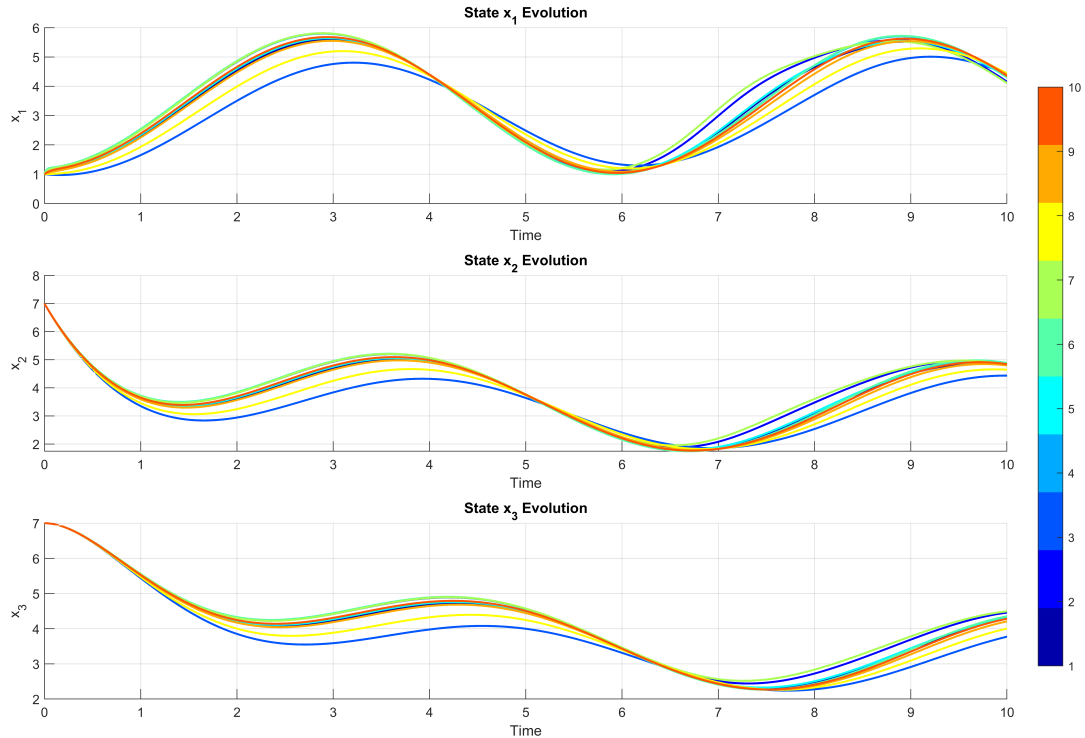


Figure 3.23: States dynamics of ten simulation with parameter uncertainties.

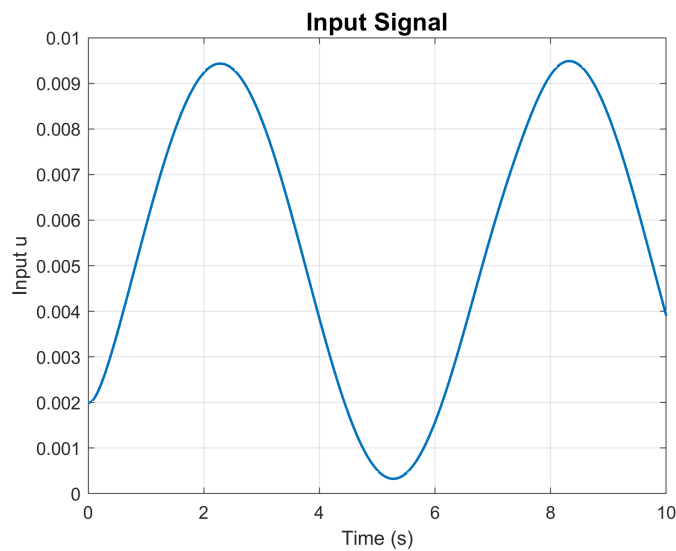


Figure 3.24: Control amplitude with uncertainty ($n=10.39$, $b=0.114$)

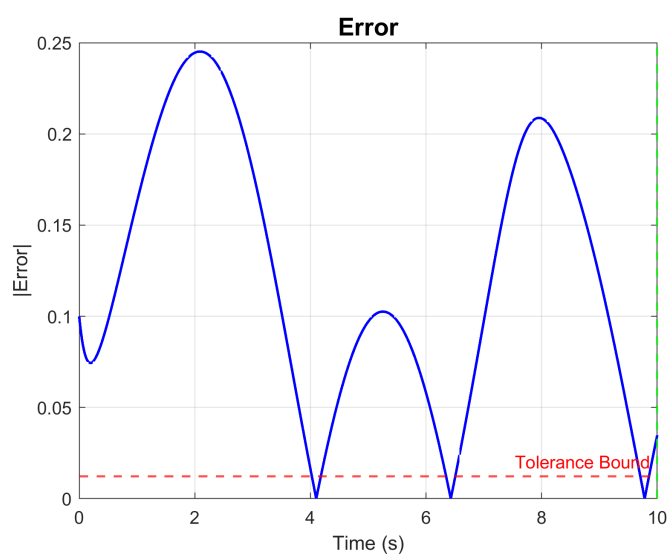


Figure 3.25: Error dynamic with uncertainty ($n=10.39$, $b=0.114$)

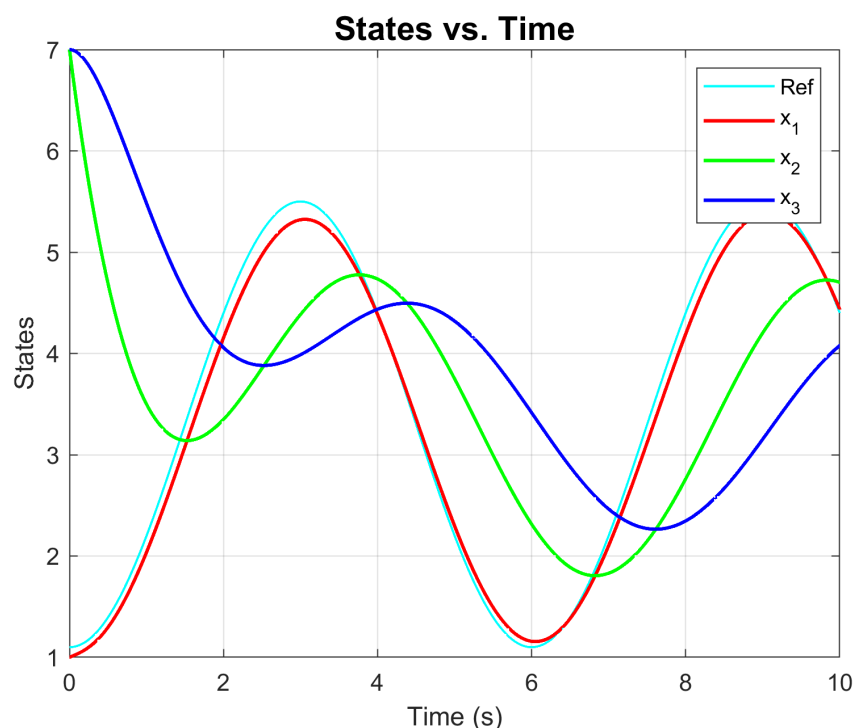


Figure 3.26: State dynamic with uncertainty ($n=10.39$, $b=0.114$)

3.4 Sliding Mode Control

The sliding-mode control (SMC) scheme can be summarized as follows:

1. **Sliding Surface Selection:** Choose a hypersurface (manifold) in the state space where the system exhibits desirable dynamics. This surface is defined such that, when the trajectory is confined to it, the system behaves in a controlled and predictable manner.
2. **Feedback Design:** Determine feedback gains so that the system's trajectory reaches (or "hits") the sliding surface in finite time and remains on it. Although the SMC law is discontinuous, this very discontinuity ensures that the transient behavior drives the trajectory to the sliding mode in finite time.

Once on the sliding surface, the system dynamics are governed by the sliding mode, which typically offers asymptotic stability towards the equilibrium. Thus, while the approach to the sliding surface is finite-time stable, the subsequent motion along the surface may be only asymptotically stable.

A key element in SMC is the *switching function*

$$\sigma : \mathbb{R}^n \rightarrow \mathbb{R}^m,$$

which measures the "distance" of the state \mathbf{x} from the sliding surface. Specifically:

$$\sigma(\mathbf{x}) \neq 0 \quad \text{if } \mathbf{x} \text{ is off the sliding surface,}$$

and

$$\sigma(\mathbf{x}) = 0 \quad \text{if } \mathbf{x} \text{ is on the sliding surface.}$$

The control law switches based on the sign of $\sigma(\mathbf{x})$, effectively applying a force that pushes the trajectory towards the surface.

Let the chosen switching function be defined as

$$\sigma = p_1(x_1 - x_d),$$

which satisfies the transversality condition.

A relevant note concerns the application of sliding-mode control (SMC) to the tracking problem of a desired sinusoidal trajectory. For the sliding to function correctly, the manifold defined by σ must be attractive for every point in the state space. This attractivity is typically demonstrated via a Lyapunov argument using the function

$$V = \frac{1}{2}\sigma^2,$$

with its derivative given by

$$\dot{V} = \sigma \dot{\sigma}.$$

In the tracking scenario, $\dot{\sigma}$ also includes a term that depends on the derivative of the reference, \dot{x}_d . The intuition to ensure convergence is to incorporate a feedforward term into the input.

Overall, the control input is given by

$$u = \frac{1}{\mathcal{L}_g(\sigma)} \left[-\mathcal{L}_f(\sigma) - k \operatorname{sgn}(\sigma) - u_{\text{FF}} \right],$$

However, in simulation it has been observed that this strategy, although rendering the manifold attractive (with $\dot{V} = -k$), does not by itself ensure the convergence on σ , as it moves in the space. Numerically, it has been found that with a sufficiently large gain k , the SMC is able to achieve the desired tracking.

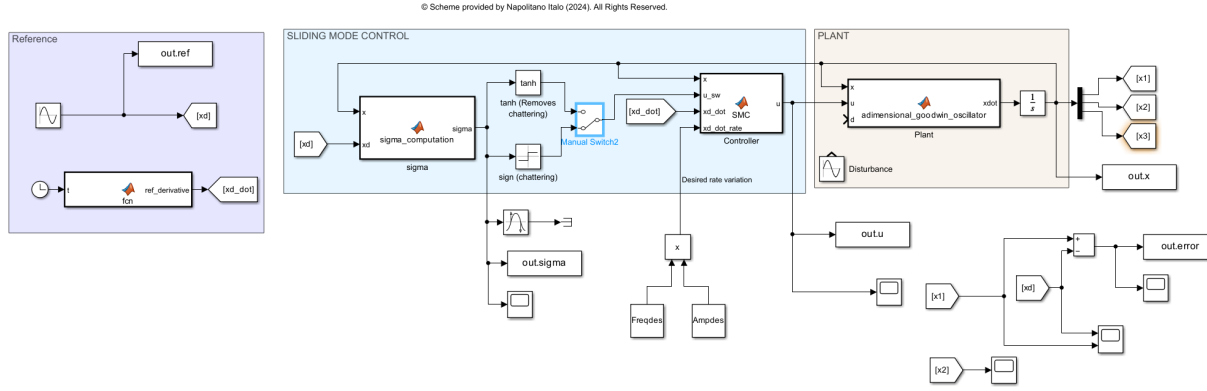


Figure 3.27: Sliding Mode Control scheme

Performance

The chosen parameters are as follows: $p_1 = 1$, $k = p_1 \cdot A \cdot F$, where A and F represent the amplitude and frequency of the reference, respectively. As before, notice that the tracking of the desired trajectory is almost perfect, meaning that in Fig. 3.29 the trajectory x_1 is overlaid on x_d .

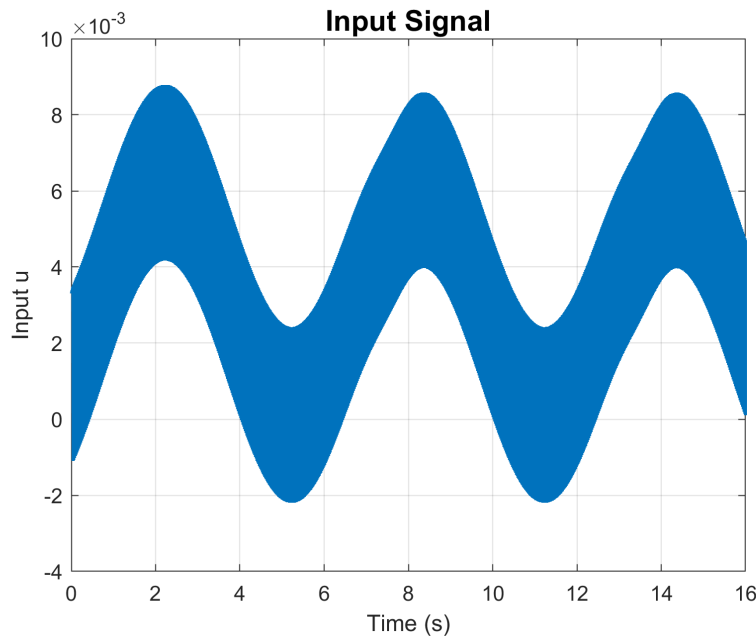


Figure 3.28: Control signal using sign function (peak: 0.0082)

For this reason, we chose to report the graphs using the hyperbolic tangent as the switching function; also remember that this chattering could damage the actuators, or be physically unfeasible.

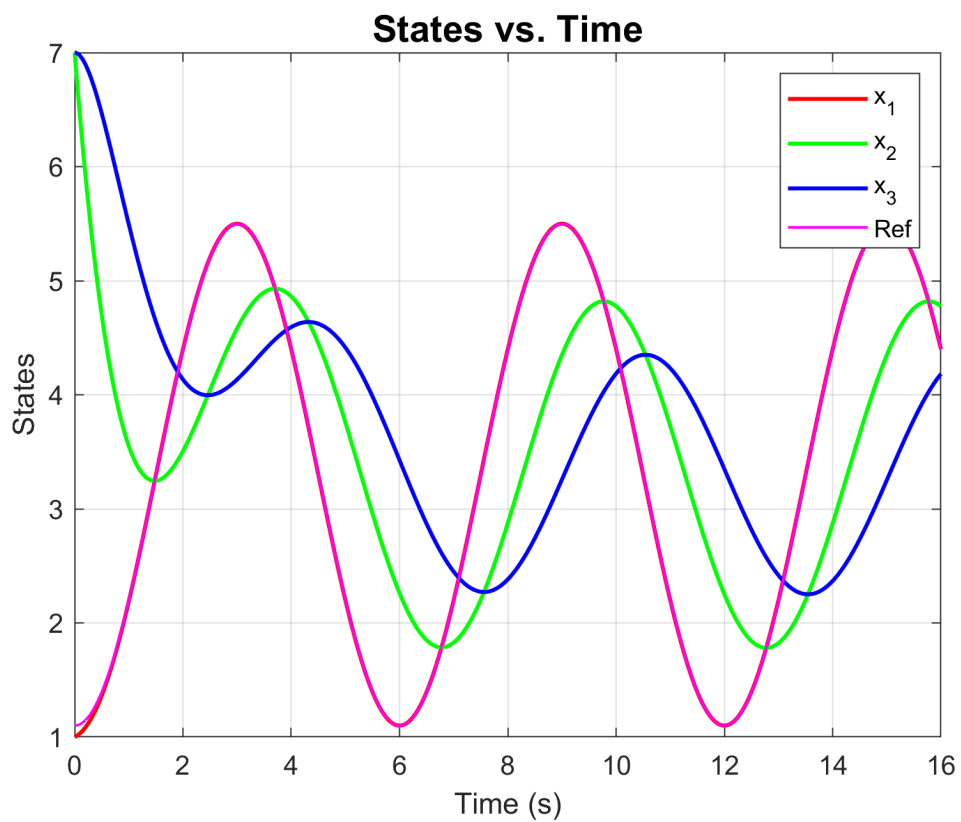


Figure 3.29: State evolution with SMC scheme

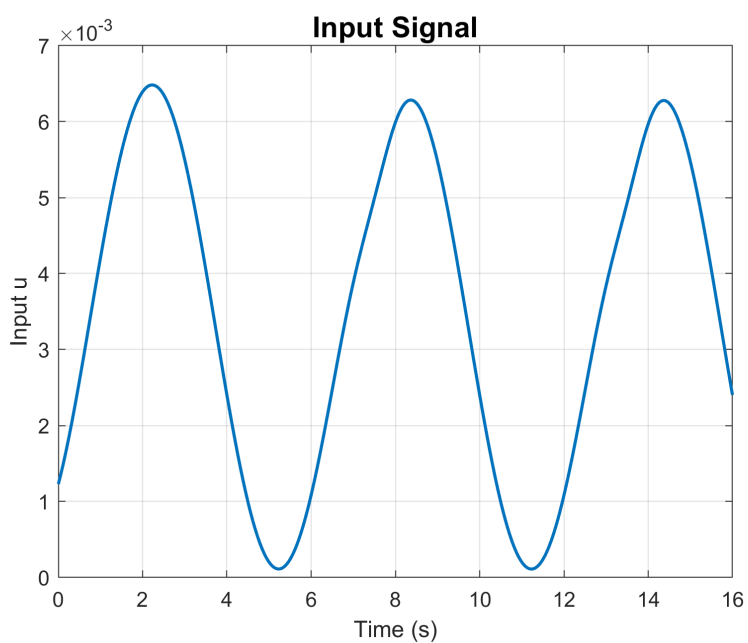


Figure 3.30: Control amplitude with SMC scheme (peak: 0.0064)

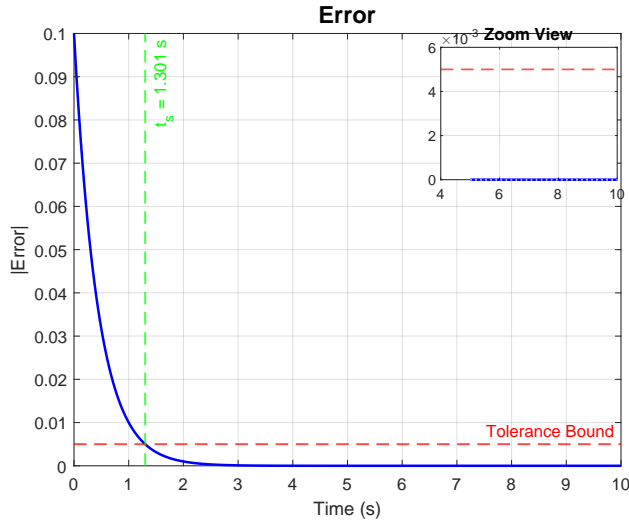


Figure 3.31: Error dynamic with SMC scheme(settling time: 1.301 seconds)

Disturbance

Disturbance has been set with an amplitude one-tenth of the desired, with a frequency a hundred times of the desired one (see Sec. 3.1 for parameters value):

$$d = \frac{A}{10} \sin(100 \cdot F \cdot t + \phi)$$

In this case, the qualitative plots are the same as before, except for the error.

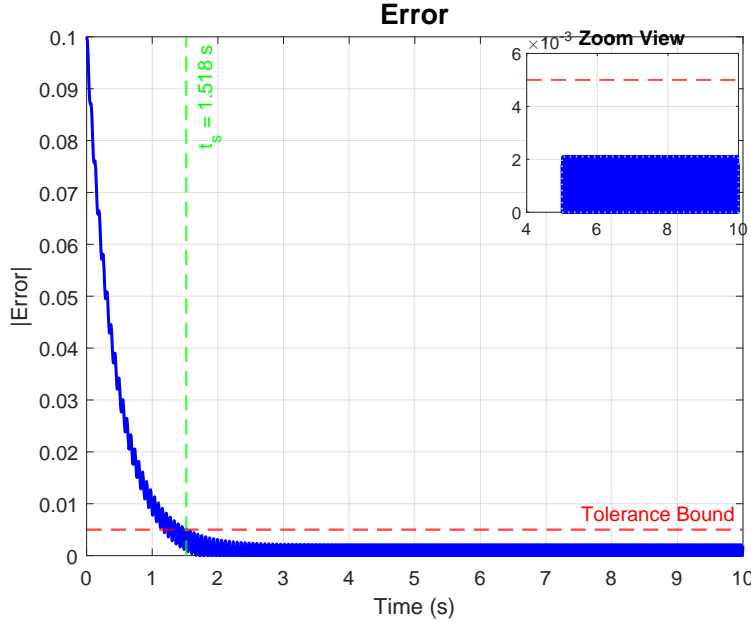


Figure 3.32: Error dynamic SMC scheme with disturbance (settling time: 1.518 seconds)

The performance is strongly influenced by the amplitude and frequency of the disturbance: at low frequencies, the error never settles (according to the given definition). It is worth noting, however, that if the sign function is used as a switching function, since it is a matched disturbance, it is perfectly rejected by the system, even for disturbances of the same amplitude as the reference. Taken as disturbance

$$d = A \sin(100 \cdot F \cdot t + \phi) + B$$

Below, the performance in the case of *sign* as switching function is shown. Perfect tracking is achieved.

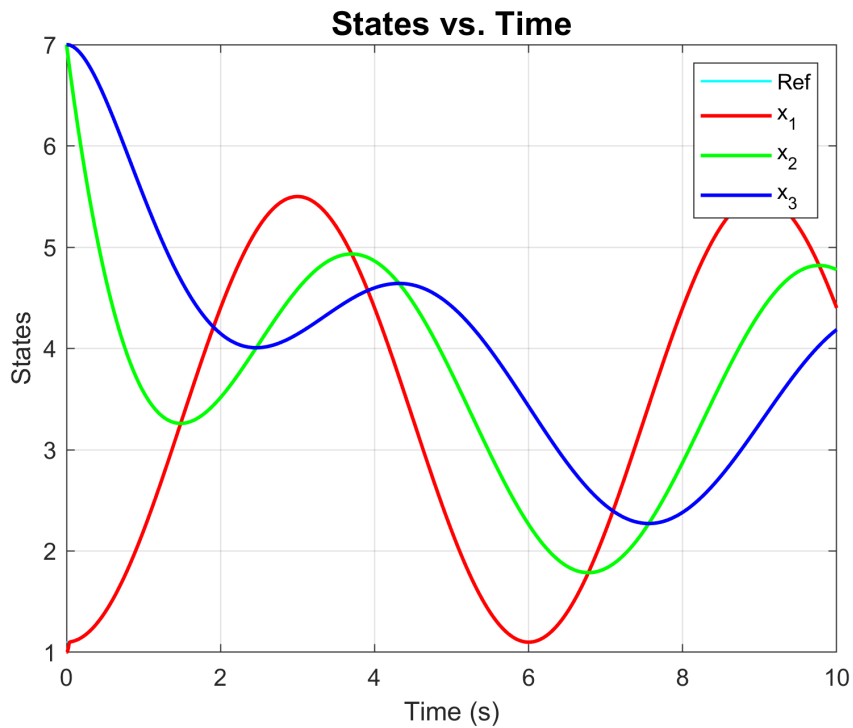


Figure 3.33: State dynamic with high disturbance with signum function

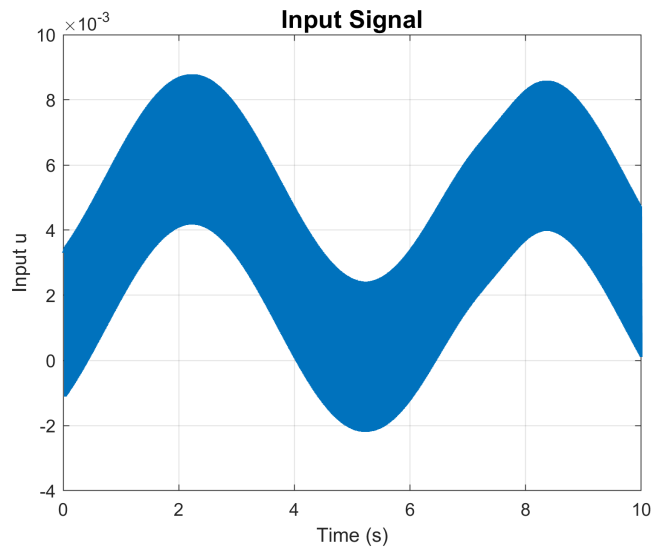


Figure 3.34: Control amplitude with high disturbance with signum function

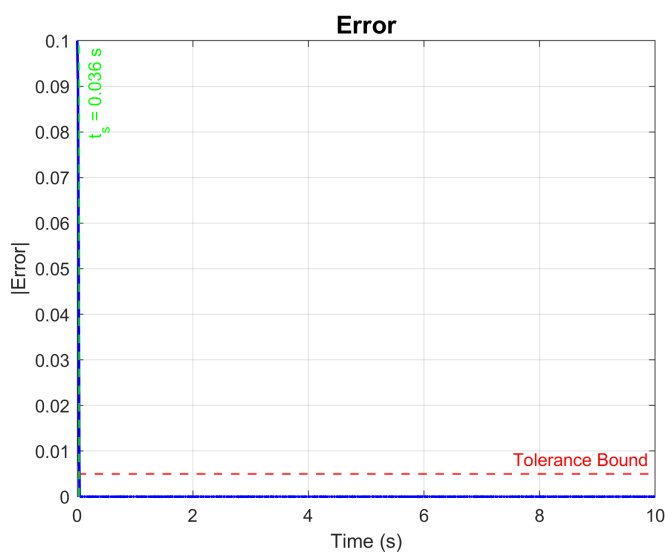


Figure 3.35: Error dynamic SMC scheme with high disturbance with signum function (settling time: 0.036 seconds)

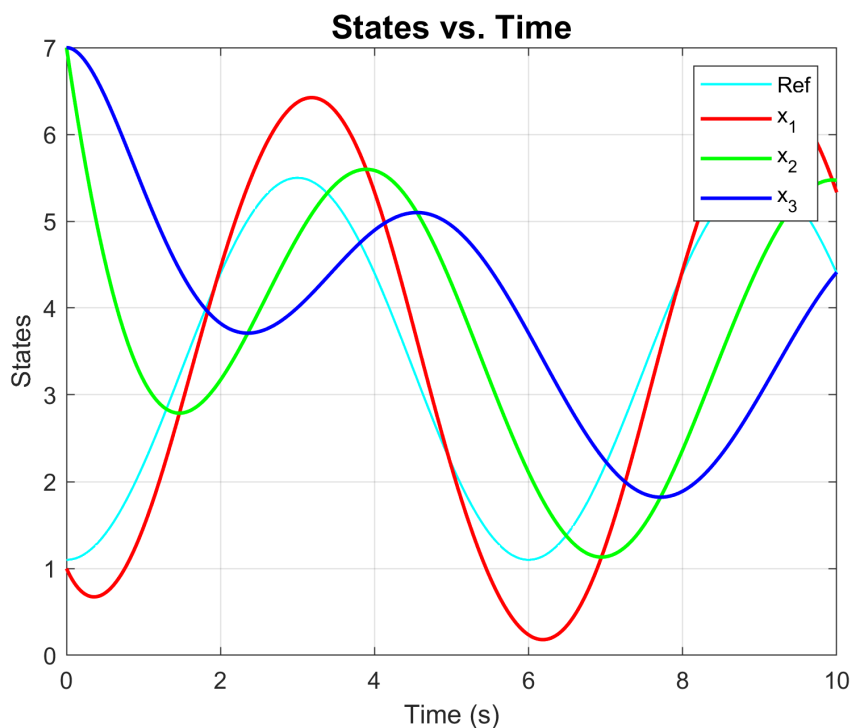


Figure 3.36: State dynamic with high disturbance with tanh function

Robustness

To check robustness of the scheme to parameter uncertainties, ten simulations have been launched, with a randomic parameter variation, up to 50% of their nominal value. Below, the state evolution in all the 10 simulations is shown, highlighting the high sensitivity to parametric variations. Finally, for one of these 10 simulations, the input and error are reported. The simulations were carried out using the hyperbolic tangent.

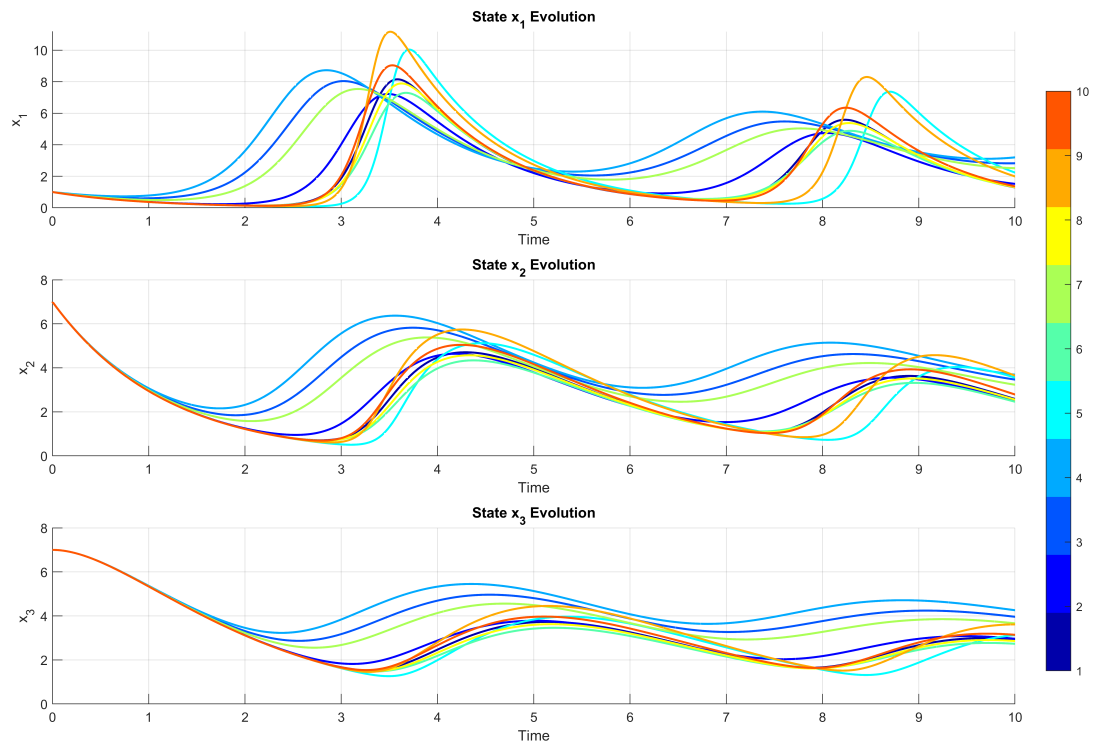
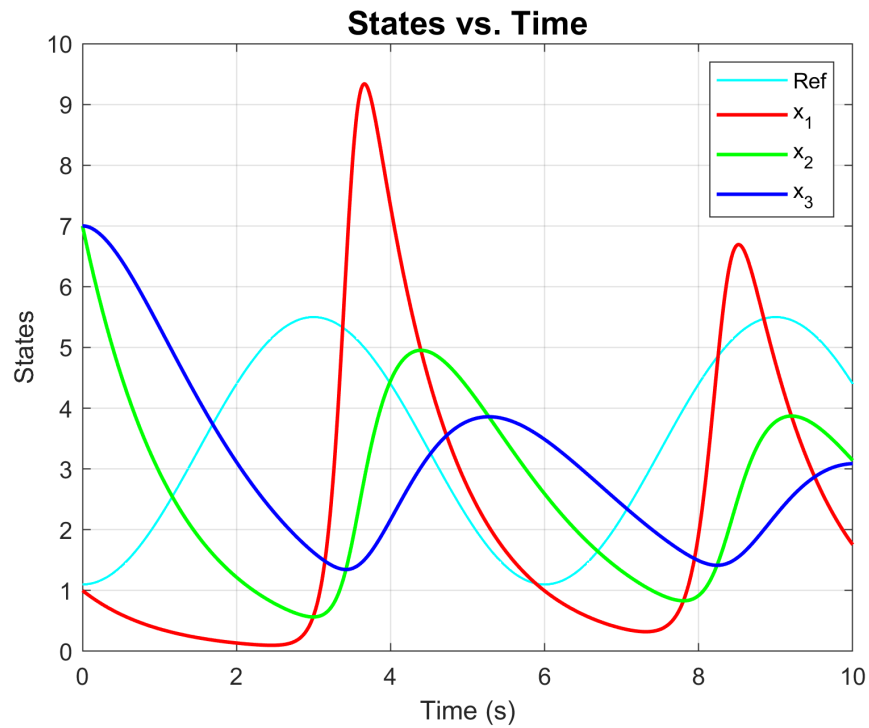
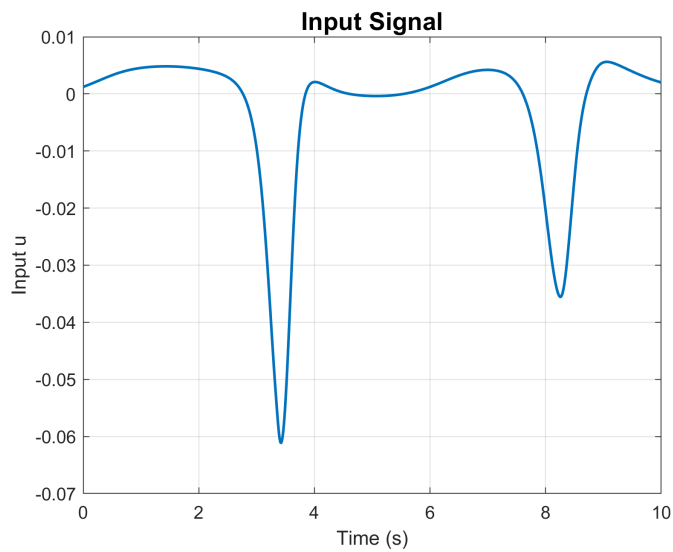


Figure 3.37: States dynamics of ten simulation with parameter uncertainties

Figure 3.38: States dynamics with uncertainty ($n=10.39$, $b=0.114$)Figure 3.39: Control amplitude with uncertainty ($n=10.39$, $b=0.114$)

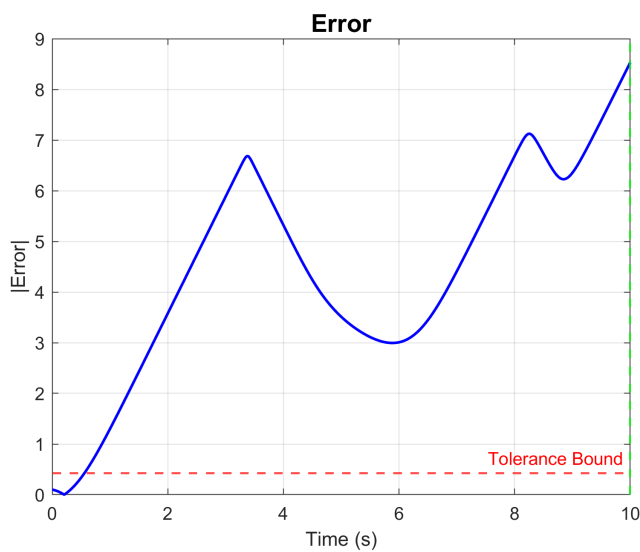


Figure 3.40: Error dynamic with uncertainty ($n=10.39$, $b=0.114$)

Chapter 4

Comparison

As shown in Table 4.1, for pure sinusoidal tracking both FBL and SMC require the same input norm (0.0064); however, FBL settles in only 0.274 s while SMC requires 1.301 s, and FBL’s error decays smoothly toward zero whereas SMC attains exact zero only after a pronounced transient. Under disturbance, FBL again outperforms SMC—settling in 0.271 s with a residual error of 0.0025 compared to SMC’s 1.518 s and 0.002 error. In the robustness test ($\pm 50\%$ parameter variation), neither controller achieves convergence, but FBL limits the steady-state error to 0.25, whereas SMC (without a discontinuous “sign” term) fails to stabilize altogether. Thus, except when using a full-strength sign action—which grants SMC perfect disturbance rejection—FBL consistently delivers faster convergence and tighter tracking in our project.

Scenario	Controller	Input norm	Settling Time [s]	Steady-State Error
Tracking	FBL	0.0064	0.274	Slowly to 0
	SMC	0.0064	1.301	0
Disturbance	FBL	0.0064	0.271	0.0025
	SMC	0.0064	1.518	0.002
Robustness	FBL	0.0092	none	0.25
	SMC	0.06	none	none

Table 4.1: Performance comparison between Feedback Linearization (FBL) and Sliding Mode Control (SMC).

Conclusion

In the Goodwin oscillator, three control techniques were tested:

1. A control attempt on the linearized system in the neighborhood of the unstable equilibrium, surrounded by the limit cycle;
2. A feedback linearization (FBL) approach, which, after globally linearizing the system, enabled the imposition of an arbitrary linear dynamic on the first state;
3. A sliding mode control (SMC) strategy, which, with appropriate modifications to classical regulation theory, allowed for the tracking of a sinusoidal trajectory.

The linearized system approach was carried out on a simplified reference, specifically designed to satisfy the criteria of local linearization; however, when interfaced with the desired reference, it proved to be an unsatisfactory strategy. In contrast, both SMC and FBL satisfied the imposed specifications, each demonstrating comparable performance with its own advantages and disadvantages. In particular, FBL tracks the reference with an error that settles one second earlier than SMC (when using a hyperbolic tangent), while both approaches share the same input amplitude.

Regarding disturbance rejection, FBL performs better than SMC. The SMC strategy was found to be very sensitive to the frequency of the incoming disturbance; however, if SMC were implemented using the signum function, it would be capable of perfectly rejecting disturbances of any amplitude, provided they are matched, as in the present case.

For the robustness analysis, a variation of up to 50% in both parameters was considered. FBL was still able to deliver acceptable performance—albeit at the expense of violating some imposed requirements—while maintaining the physical feasibility of the problem. In contrast, SMC was highly sensitive to parameter variations: its control effect almost vanished, reverting to the open-loop dynamics.

Bibliography

- [1] Wikipedia contributors. *Circadian rhythm — Wikipedia, The Free Encyclopedia*. 2025. URL: https://en.wikipedia.org/wiki/Circadian_rhythm.
- [2] Yan Xu et al. “Goodwin oscillator model explains different response of circadian rhythms to constant light”. In: *Physica A: Statistical Mechanics and its Applications* 618 (2023), p. 128711. ISSN: 0378-4371. DOI: <https://doi.org/10.1016/j.physa.2023.128711>. URL: <https://www.sciencedirect.com/science/article/pii/S0378437123002662>.